Robustness Analysis and Optimally Robust Control Design via Sum-of-Squares

Andrei Dorobantu*
Department of Aerospace Engineering & Mechanics
University of Minnesota, Minneapolis, MN, 55455, USA

Luis G. Crespo†
National Institute of Aerospace, Hampton, VA, 23666, USA

Peter J. Seiler‡
Department of Aerospace Engineering & Mechanics
University of Minnesota, Minneapolis, MN, 55455, USA

A control analysis and design framework is proposed for systems subject to parametric uncertainty. The underlying strategies are based on sum-of-squares (SOS) polynomial analysis and nonlinear optimization to design an optimally robust controller. The approach determines a maximum uncertainty range for which the closed-loop system satisfies a set of stability and performance requirements. These requirements, defined as inequality constraints on several metrics, are restricted to polynomial functions of the uncertainty. To quantify robustness, SOS analysis is used to prove that the closed-loop system complies with the requirements for a given uncertainty range. The maximum uncertainty range, calculated by assessing a sequence of increasingly larger ranges, serves as a robustness metric for the closed-loop system. To optimize the control design, nonlinear optimization is used to enlarge the maximum uncertainty range by tuning the controller gains. Hence, the resulting controller is optimally robust to parametric uncertainty. This approach balances the robustness margins corresponding to each requirement in order to maximize the aggregate system robustness. The proposed framework is applied to a simple linear short-period aircraft model with uncertain aerodynamic coefficients.

I. Introduction

Classical control design is typically focused on satisfying a set of closed-loop stability and performance requirements with sufficient margins of robustness to model uncertainty. These requirements vary depending on the application, but are generally based on the same fundamental principles. For example, while the required level of robustness is different in every problem, the effect of model uncertainty must always be evaluated. Typical requirements provide specifications for stability, command tracking, disturbance rejection, noise attenuation, and transient response.

Current practices in control design verification rely on classical robustness analysis of linearized system dynamics obtained over a set of operating points. Monte Carlo simulations of the non-linear dynamics are used to check for any oversights. If the requirements are not satisfied, the controller is tuned through an ad-hoc process and control verification is repeated. This process is inefficient and may result in overly conservative designs. Advanced robust control techniques, such as mu-synthesis,[1] were formulated to include model

*PhD Candidate, AIAA Student Member
†Associate Research Fellow, AIAA Member
‡Assistant Professor, AIAA Member

uncertainty as part of the design process. These techniques yield optimal designs by explicitly accounting for model uncertainty and performance requirements. However, they typically produce conservative, high-order, and unstructured controllers. Further, standard techniques cannot implement multiple requirements without constructing a vector valued problem, which can lead to increasingly conservative results. The approach proposed in this paper incorporates some of the optimality features of advanced robust control into a classical design framework by targeting real parametric uncertainty.

The framework applies sum-of-squares (SOS) polynomial analysis[2] in sequence with a nonlinear optimization. Given a set of controller gains, the uncertainty analysis problem is solved using an SOS algorithm. An SOS optimization proves that the closed-loop system complies with the requirements for a specified range of uncertainty. The maximum uncertainty range, calculated by assessing a sequence of increasingly larger ranges, serves as a robustness metric for the closed-loop system. This metric is a numerically proven lower bound on the true uncertainty range for which the closed-loop system is requirement compliant. Standard nonlinear optimization is not applicable to this analysis because convergence to a globally optimal result would not be guaranteed. The control design problem, however, lends itself to nonlinear optimization. This optimization tunes the controller gains in order to enlarge the maximum uncertainty range. Optimal gains are identified that maximize robustness in the closed-loop system. Additional details on related control analysis and design approaches are available in References 3 and 4.

The proposed framework assumes a fixed controller structure and polynomial stability and performance requirements. These requirements, which are defined as inequality constraints on several stability and performance metrics, are restricted to depend polynomially on the uncertainty. However, this dependency often arises naturally when considering stability and frequency domain requirements for linear time-invariant (LTI) systems. The framework is applied to a linear short-period aircraft model with uncertain aerodynamic coefficients. This simple example has been chosen to facilitate the reproducibility and interpretation of results.

Remaining sections of this paper are organized as follows. Section II describes a linear short-period aircraft model with parametric uncertainty. A classical controller is designed to increase damping and to achieve reference tracking in the nominal closed-loop system. Section III derives the set of stability and performance requirements to be satisfied. Section IV briefly introduces SOS analysis and describes its usage within the proposed strategies. Section V presents the optimally robust control design formulation. Finally, Section VI offers some concluding remarks.

II. Aircraft Model and Controller

An example of a linear short-period aircraft model with uncertain aerodynamic coefficients[5] is described in this section. A classical flight controller is designed for the nominal system to increase damping and to achieve reference tracking. The controller is manually tuned to satisfy traditional damping, tracking, rise-time, and noise attenuation specifications, as well as gain and phase robustness margins. Although the design appears satisfactory in the traditional sense, the remaining sections are used to assess and improve the robustness of this controller to parametric uncertainty.

A. Short-Period Aircraft Model

The X-15 was an experimental hypersonic rocket propelled aircraft flown by NASA in the 1960s. A short-period model of its longitudinal dynamics is given by the following system:

$$\dot{x} = A(\boldsymbol{\lambda})x + Bu \tag{1}$$

The states of this system are angle-of-attack α (deg) and pitch rate q (deg/sec), given by $x = [\alpha,\ q]^\top$. The input to the system is elevator deflection $u = \delta_e$ (deg). The vector $\boldsymbol{\lambda}$ denotes parametric uncertainty. State and input matrices for the X-15 short-period model are defined as follows:

$$A(\boldsymbol{\lambda}) = \begin{bmatrix} a_1 & a_2 \\ a_3(1+\lambda_\alpha) & a_4(1+\lambda_q) \end{bmatrix} = \begin{bmatrix} -0.2950 & 1 \\ -13.0798(1+\lambda_\alpha) & -0.2084(1+\lambda_q) \end{bmatrix} \tag{2}$$

$$B = \begin{bmatrix} 0 \\ b_1 \end{bmatrix} = \begin{bmatrix} 0 \\ -9.4725 \end{bmatrix} \tag{3}$$

The terms λ_α and λ_q in the aircraft model represent real parametric uncertainty in the aerodynamic coefficients C_{m_α} and C_{m_q}, respectively.[1,6] The nominal system is given by $\lambda_\alpha = \lambda_q = 0$. Thus, the nominal uncertain parameter is $\bar{\boldsymbol{\lambda}} = [0, 0]$. As an example, 75% uncertainty is considered by allowing each uncertain parameter to vary on the interval $[-.75\ \ .75]$. Eigenvalue decomposition reveals that the nominal short-period dynamics have a damping ratio $\zeta = 0.07$ and a natural frequency $\omega_n = 3.63$ rad/sec. Hence, the dynamics are lightly damped. One of the goals of the control design is to attenuate oscillations corresponding to this dynamic mode.

A family of transfer functions is generated by gridding the uncertainty parameters over the uncertainty range $[-.75\ \ .75] \times [-.75\ \ .75]$. This illustrates the effect of uncertainty on the open-loop dynamics. Figure 1 shows the frequency response for this family of transfer functions from the elevator input δ_e to the angle-of-attack output α. The nominal model, corresponding to $\bar{\boldsymbol{\lambda}}$, is highlighted by the darker curve. The uncertainty causes frequency responses to group into clusters by λ_α, and variations within each cluster are due to λ_q. Hence, the open-loop dynamics are more sensitive to variations in λ_α than in λ_q.

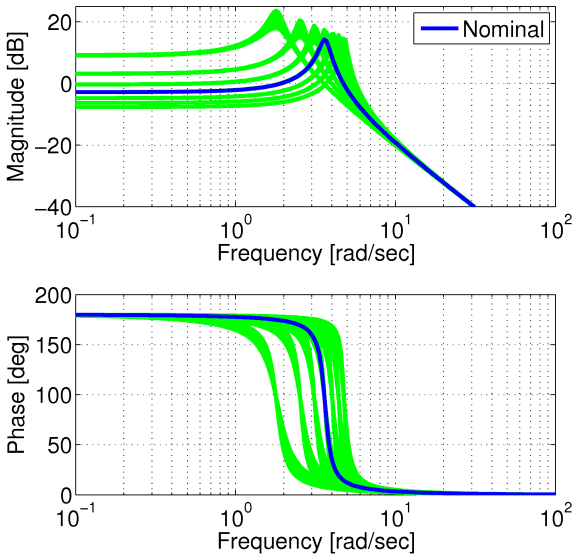

Figure 1. Family of open-loop transfer functions from δ_e to α with 75% uncertainty.

Next, a classical flight controller for the nominal aircraft model is designed using a standard approach. The design takes into consideration desired performance characteristics related to damping, tracking, rise-time, and noise attenuation, as well as gain and phase robustness margins.

B. Controller

An inner-loop proportional (P) controller is implemented with pitch rate feedback to increase damping in the short-period oscillation. An outer-loop proportional-integral (PI) controller is implemented with angle-of-attack feedback to achieve reference tracking of the signal r at low frequency. The closed-loop control architecture is illustrated by the following block diagram:

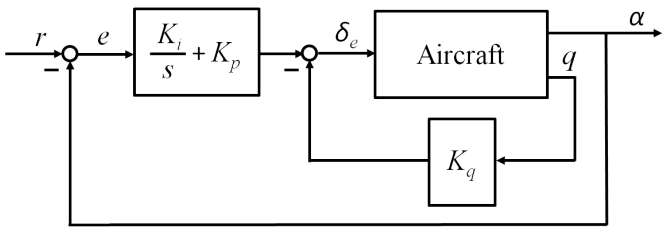

Figure 2. Closed-loop system interconnection.

The overall control architecture is governed by three gains: K_q, K_p, and K_i. Proportional rate feedback is a common approach to increasing damping in aircraft dynamics. An inner-loop proportional gain $K_q = -1$ is selected. The resulting nominal inner-loop system is overdamped with real poles at -2 and -7.98. Robustness of the inner-loop is characterized by an infinite gain margin and a phase margin of 91.46 degrees.

An outer-loop controller is designed around the inner-loop system using the principles of loopshaping. The objective is to track a reference angle-of-attack command. Therefore, the loop gain is boosted at low frequency using integral action. The gain $K_p = -1$ is fixed to ensure that the PI controller only has integral effect on the loop transfer function at low frequency. An integral gain $K_i = -2$ is selected to obtain a rise time of 2 seconds, no overshoot, and zero steady-state error. Overall, the bandwidth of the closed-loop system is decreased significantly from 5 rad/sec in the open-loop to 1 rad/sec in the closed-loop.

Robustness of the outer-loop system, evaluated at the input of the aircraft model, is characterized by an infinite gain margin and a phase margin of 89.19 degrees. Clearly, closed-loop robust stability is not a great concern. Instead, the control challenge is focused on performance in the presence of uncertainty. Figure 3 shows the performance characteristics of the nominal controller, as well as the effect of uncertainty on the closed-loop dynamic. Samples of uncertainty parameter pairs are drawn from the 75% range.

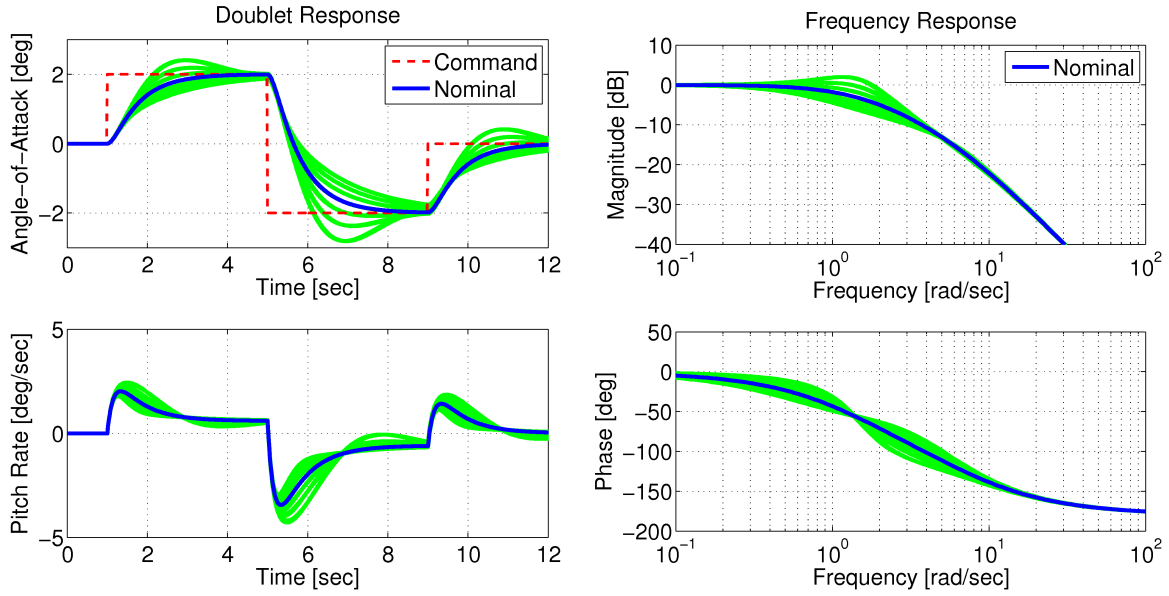

(a) Family of doublet responses.

(b) Family of frequency responses from r to α.

Figure 3. Properties of the closed-loop dynamics with 75% uncertainty.

Figure 3 highlights properties of the closed-loop system. Time domain characteristics of the nominal system, such as a 2 second rise time and no overshoot, are confirmed by the plot on the left. Frequency domain characteristics of the closed-loop transfer function, such as reference tracking and bandwidth, are shown in the plot on the right. Figure 3 also graphically represents the effect of uncertain aerodynamic coefficients on the closed-loop dynamics. Both time domain and frequency domain perspectives indicate that uncertainty primarily affects closed-loop damping.

Classical time and frequency domain analysis indicate that the nominal control design above meets standard performance and robustness characteristics. This nominal controller, defined by the three gains K_q, K_p, and K_i, is denoted $\boldsymbol{k}_{nom} = [-1, -1, -2]$.

III. Stability and Performance Constraints

Stability and performance requirements for the closed-loop system are described next. Stability in the presence of parametric model uncertainty is a key robustness requirement that must be satisfied. Performance requirements related to reference tracking, rise time, overshoot, and noise attenuation are formulated to formalize the desired closed-loop behavior. Requirements are defined as inequality constraints. These constraints depend on the uncertainty $\boldsymbol{\lambda}$ and the controller gain $\boldsymbol{k}$. When the constraints, denoted $g_i(\boldsymbol{\lambda}, \boldsymbol{k}) \leq 0$,

are satisfied for all i, the requirements are satisfied as well. The uncertain parameter realizations for which the requirements are satisfied are given by $\mathcal{S} = \{\boldsymbol{\lambda} : g_i(\boldsymbol{\lambda}, \boldsymbol{k}) \leq 0 \text{ for all } i\}$.

Robust stability is specified through a set of constraints that depend on coefficients in the characteristic polynomial of the closed-loop system. The outer loop transfer function, from signal e to α and denoted $L(s)$, is derived algebraically using the system interconnection in Figure 2, the aircraft model, and the controller gains. An analytic representation of the outer loop transfer function is given by the following:

$$L(s) = \frac{N_1 s + N_2}{s^3 + D_1 s^2 + D_2 s} \tag{4}$$

where

$$\begin{aligned} N_1 &= a_2 b_1 K_p \\ N_2 &= a_2 b_1 K_i \\ D_1 &= -a_1 - a_4(1 + \lambda_q) + b_1 K_q \\ D_2 &= a_1 a_4 (1 + \lambda_q) - a_1 b_1 K_q - a_2 a_3 (1 + \lambda_\alpha) \end{aligned}$$

Stability is enforced through constraints derived analytically by construction of the Routh-Hurwitz array.[7] The Routh-Hurwitz array depends on coefficients in the characteristic polynomial of the closed-loop system, and provides parameter dependent inequality constraints for stability. The characteristic polynomial is given by the following relationship:

$$0 = 1 + L(s) \tag{5}$$

$$0 = s^3 + D_1 s^2 + (D_2 + N_1)s + N_2 \tag{6}$$

Satisfying the Routh-Hurwitz inequality constraints over the uncertain parameter space determines a region of robust stability. The stability requirement functions are shown in Equations (7 - 10). Alternative approaches to describe robust stability are available.[8]

$$g_1(\boldsymbol{\lambda}, \boldsymbol{k}) = -D_1 \tag{7}$$

$$g_2(\boldsymbol{\lambda}, \boldsymbol{k}) = -D_2 - N_1 \tag{8}$$

$$g_3(\boldsymbol{\lambda}, \boldsymbol{k}) = -N_2 \tag{9}$$

$$g_4(\boldsymbol{\lambda}, \boldsymbol{k}) = -D_1(D_2 + N_1) + N_2 \tag{10}$$

Performance requirements are enforced by specifying limits at particular frequencies on the magnitude of the outer loop transfer function. This approach to control design is often known as loopshaping. It is possible to enforce each performance constraint over a range of frequencies. For simplicity in this analysis, however, each requirement on the loop transfer function is prescribed at a single frequency point.

To ensure adequate reference tracking, the loop gain is lower bounded by $c_5 = 10$ at $\omega_5 = 0.7$ rad/sec. Noise attenuation is achieved by upper bounding the loop gain by $c_6 = 0.01$ at $\omega_6 = 40$ rad/sec. Further, the closed-loop response should have a bandwidth near 1 rad/sec and exhibit low overshoot. These requirements imply that the outer loop transfer function should cross-over near 1 rad/sec, and that its slope should be no lower than -30 dB/dec near that frequency. The slope limit is drawn from the Bode Gain-Phase formula to ensure a satisfactory phase margin. In this case, however, it also ensures low overshoot. To satisfy the cross-over and slope limits, the loop transfer function is upper bounded by $c_7 = \sqrt{15}$ at $\omega_7 = 1/\sqrt{10}$ rad/sec and lower bounded by $c_8 = 1/\sqrt{15}$ at $\omega_8 = \sqrt{10}$ rad/sec.

The performance constraints must be expressed as polynomial inequalities for the application of SOS analysis. When evaluated at $s = j\omega$, the magnitude squared of $L(j\omega)$ is given by Equation (11). The numerator and denominator have been split into their real and imaginary parts, and then squared.

$$|L(j\omega)|^2 = \frac{(N_1\omega)^2 + (N_2)^2}{(-\omega^3 + D_2\omega)^2 + (-D_1\omega^2)^2} \tag{11}$$

Each performance constraint is adapted to this format. Equations (12 - 15) show the requirement functions

associated with the performance requirements:

$$g_5(\boldsymbol{\lambda}, \boldsymbol{k}) = -[(N_2)^2 + (N_1\omega_5)^2] + c_5^2[(-D_1\omega_5^2)^2 + (-\omega_5^3 + D_2\omega_5)^2] \tag{12}$$

$$g_6(\boldsymbol{\lambda}, \boldsymbol{k}) = \quad [(N_2)^2 + (N_1\omega_6)^2] - c_6^2[(-D_1\omega_6^2)^2 + (-\omega_6^3 + D_2\omega_6)^2] \tag{13}$$

$$g_7(\boldsymbol{\lambda}, \boldsymbol{k}) = \quad [(N_2)^2 + (N_1\omega_7)^2] - c_7^2[(-D_1\omega_7^2)^2 + (-\omega_7^3 + D_2\omega_7)^2] \tag{14}$$

$$g_8(\boldsymbol{\lambda}, \boldsymbol{k}) = -[(N_2)^2 + (N_1\omega_8)^2] + c_8^2[(-D_1\omega_8^2)^2 + (-\omega_8^3 + D_2\omega_8)^2] \tag{15}$$

Every inequality constraint $g_i(\boldsymbol{\lambda}, \boldsymbol{k})$ is a function of the two uncertainty parameters in $\boldsymbol{\lambda}$ and the three controller gains in $\boldsymbol{k}$. The region of requirements satisfaction $\mathcal{S}$ for any fixed controller is represented by the intersection of the sets $g_i(\boldsymbol{\lambda}, \boldsymbol{k}) \leq 0$ in the uncertain parameter space. This region indicates all admissible parametric model uncertainty pairs that satisfy the requirements. Figure 4 on the left shows $\mathcal{S}$ for the nominal controller as the unshaded region. The region of requirements violation is shaded. The nominal controller satisfies all the requirements at the nominal value of uncertainty at the origin. Constraint function $g_7(\boldsymbol{\lambda}, \boldsymbol{k_{nom}})$, which primarily varies with λ_α, is dominant in the vicinity of the origin. On the right is the corresponding Bode magnitude plot of the nominal outer loop transfer function along with control points that prescribe the performance requirements. Although each constraint marker is over-sized for emphasis, the control point occurs precisely at the marker center.

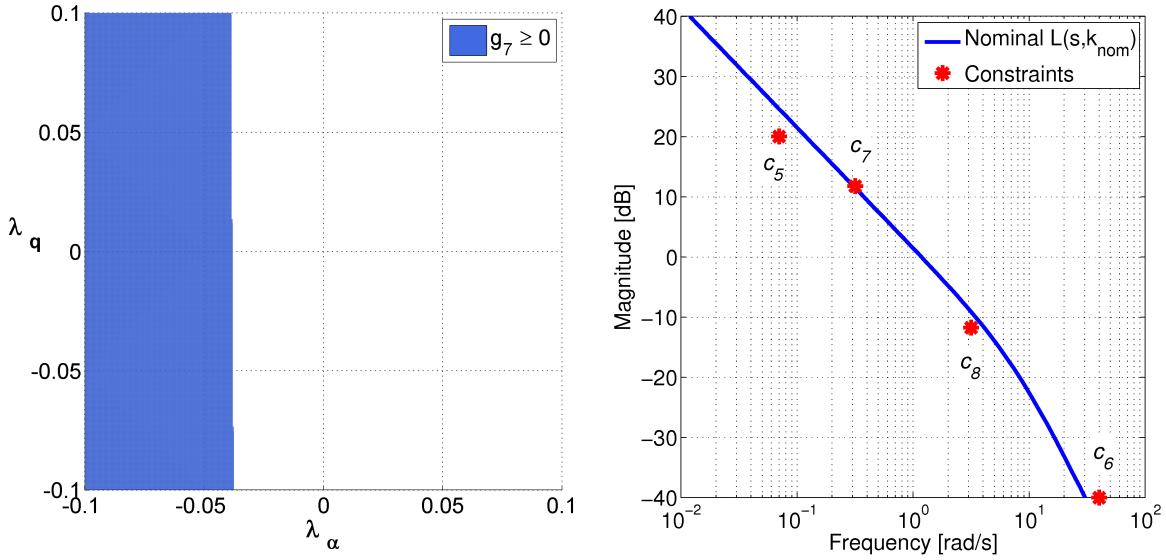

(a) Requirement satisfaction region $\mathcal{S}$ and its complement. (b) Nominal outer loop transfer function with constraints.

Figure 4. Graphical representation of performance and robustness requirements.

The ability of the controller to satisfy the requirements in the presence of uncertainty is examined next. One approach entails locating the point along the requirements violation boundary that is closest to the nominal parameter point. A ball centered at $\bar{\boldsymbol{\lambda}}$ having this distance as its radius defines a range of uncertainties for which all the requirements are satisfied. However, solving this problem using nonlinear optimization is unreliable because convergence to the global minimum distance cannot be guaranteed. In other words, the nonlinear optimization may converge to a non-global minimum along the requirements violation boundary, which would falsely indicate too large a region of compliance. The resulting uncertainty set would be flawed since it could contain elements for which the closed-loop system violates a constraint.

The next section describes a formally verifiable SOS optimization to identify a range of uncertainties for which the closed-loop system is requirement compliant. The analysis is formulated as a convex optimization problem, which guarantees a globally optimal result. However, SOS optimization has several significant drawbacks. The computational complexity of the problem grows rapidly with the number of uncertain parameters and the polynomial degree of the requirements. Further, all system dynamics and constraints are restricted to polynomial functions. Despite these challenges, SOS analysis can be successfully applied to control systems of moderate size.

IV. Sum-of-Squares Optimization

Sum-of-squares (SOS) optimization is used to determine if, given a fixed set of controller gains $\boldsymbol{k}$, the requirements are satisfied in a region of the uncertain parameter space. For simplicity in the presentation, the single constraint SOS optimization is considered first. If $g(\boldsymbol{\lambda})$ is a polynomial of degree less than or equal to $2d$ in the variable $\boldsymbol{\lambda} \in \mathbb{R}^v$, where v is the number of uncertain parameters, its vectorial representation is

$$g(\boldsymbol{\lambda}) = \boldsymbol{c}^\top \boldsymbol{x}(\boldsymbol{\lambda}) \tag{16}$$

where $\boldsymbol{x}$ is a vector of monomials in $\boldsymbol{\lambda}$ of degree less than or equal to $2d$, and $\boldsymbol{c}$ is a vector of coefficients. Equivalently, the Gram matrix representation of this polynomial is

$$g(\boldsymbol{\lambda}) = \boldsymbol{z}^\top(\boldsymbol{\lambda}) Q \boldsymbol{z}(\boldsymbol{\lambda}) \tag{17}$$

where $\boldsymbol{z}$ is a vector of monomials in $\boldsymbol{\lambda}$ of degree less than or equal to d, and Q is a symmetric matrix. The Gram representation of $g(\boldsymbol{\lambda})$ is not unique, and all possible representations can be parametrized. Define the linear operator $\mathcal{L}$ that maps each symmetric matrix Q to the polynomial coefficients in $\boldsymbol{c}$:

$$\mathcal{L}(Q) = \boldsymbol{c} \tag{18}$$

A matrix representation of $\mathcal{L}$ can be computed since both its domain and its range are finite dimensional. This transformation enables the parameterization of the family of symmetric matrices yielding Gram representations via:

$$Q = Q_0 + \sum_{i=1}^{m} \boldsymbol{p}_i N_i \tag{19}$$

where Q_0 is the symmetric matrix corresponding to a particular Gram representation (i.e., $\mathcal{L}(Q_0) = \boldsymbol{c}$), the set $\{N_1, \ldots N_m\}$ is a basis of the null space of $\mathcal{L}$ (i.e., $\mathcal{L}(N_i) = 0$ for $i = 1, \ldots, m$), and $\boldsymbol{p}$ is a vector of multipliers. Note that any value of $\boldsymbol{p}$ in Equation (19) yields a valid Gram representation of $g(\boldsymbol{\lambda})$.

The Gram representation of a polynomial is used to determine whether a polynomial is a sum-of-squares (SOS). In general, the polynomial $g(\boldsymbol{\lambda})$ is a SOS if there exist polynomials $h_1, \ldots, h_n$ such that $g(\boldsymbol{\lambda}) = \sum_{i=1}^{n} h_i^2$. A key property of SOS polynomials is that they are globally positive semi-definite. Further, the polynomial $g(\boldsymbol{\lambda})$ is a SOS if and only if there exists a positive semi-definite matrix Q, denoted $Q \succeq 0$, that satisfies Equation (17).[2,9] The functions $h_1, \ldots, h_n$ that constitute the SOS representation of $g(\boldsymbol{\lambda})$ result from making Choleski or Schur decompositions of Q. Consequently, $g(\boldsymbol{\lambda})$ is a SOS if and only if there exists a $\boldsymbol{p}$ for which $Q_0 + \sum_{i=1}^{m} \boldsymbol{p}_i N_i \succeq 0$. Hence, the question of whether a polynomial is a SOS reduces to a Linear Matrix Inequality (LMI) feasibility problem.

Numerical techniques for solving semi-definite programs can be used to find a solution to this LMI feasibility problem. Publicly available software, such as SOSTOOLS,[10] SOSOPT,[11] YALMIP[12] and SeDuMi[13,14] automate the process of posing and solving this convex optimization. Unfortunately, its computational requirements (e.g. the number of monomials that require representation and the dimension of the null space) grow rapidly with the degree of the polynomials and the dimension of the parameter space v. For this analysis, SOSOPT along with SeDuMi are used for the SOS optimization.

Given a system subject to parametric uncertainty, and a controller with gains $\boldsymbol{k}$, it is desired to determine if the closed-loop system satisfies a set of requirements for a range of uncertainty. The uncertainty range is defined as $\mathcal{E}(\boldsymbol{\lambda}) \subseteq \mathbb{R}^v$. SOS optimization is used to numerically prove that $\mathcal{E}(\boldsymbol{\lambda})$ (with a polynomial boundary) is contained in the requirement satisfaction region $\mathcal{S}$. The set containment problem is evaluated using the following Theorem:[15]

Theorem 1 *Assume $e(\boldsymbol{\lambda}, \bar{\boldsymbol{\lambda}}, r)$ is a polynomial function. Let $\mathcal{E}(\boldsymbol{\lambda}, r) = \{\boldsymbol{\lambda} : e(\boldsymbol{\lambda}, \bar{\boldsymbol{\lambda}}, r) \leq 0\}$ be a closed set whose volume is proportional to $r > 0$ and has $\bar{\boldsymbol{\lambda}}$ as its geometric center. If there exist a function $q(\boldsymbol{\lambda})$ such that $q(\boldsymbol{\lambda}) \geq 0$ and $q(\boldsymbol{\lambda}) e(\boldsymbol{\lambda}, \bar{\boldsymbol{\lambda}}, r) - g(\boldsymbol{\lambda}) \geq 0$ for all $\boldsymbol{\lambda}$, then $\mathcal{E}(\boldsymbol{\lambda}, r) \subseteq \mathcal{S}$.*

Theorem 1 can be generalized for multiple constraint functions $g_i(\boldsymbol{\lambda})$. Note that there are 2 positive semi-definite (PSD) conditions per constraint function. PSD conditions are numerically difficult to solve. However, by restricting the constraint functions $g_i(\boldsymbol{\lambda})$ to be polynomials, and by altering the PSD conditions in Theorem 1 to be SOS conditions, set containment can be established efficiently. While all SOS polynomials are PSD, not all the PSD polynomials are SOS. Therefore, satisfying SOS conditions is sufficient to prove

the global non-negativity of the conditions in Theorem 1. In practice, the SOS polynomial multipliers $q_i(\boldsymbol{\lambda})$ must be restricted to be in a fixed finite dimensional subspace of polynomials (e.g., quadratic polynomials). This is achieved by prescribing a polynomial basis and using semi-definite programing to search for the coefficients of the corresponding linear combination.

SOS optimization is used to determine if $\mathcal{E}(\boldsymbol{\lambda}, r) \subseteq \mathcal{S}$ for a fixed value of r. A bisection algorithm is used to determine the largest r for which this condition holds. This yields a numerically proven lower bound on the radius leading to a requirement violation. If r^* is the resulting radius, the corresponding uncertainty set, $\mathcal{E}(\boldsymbol{\lambda}, r^*)$, is called the *Maximal Set*. Note that r^* is a margin of robustness that indicates the separation between the nominal parameter point $\bar{\boldsymbol{\lambda}}$ and the requirement violation region. While the LMI feasibility problem searches over the coefficients of the polynomial multipliers of $q_i(\boldsymbol{\lambda})$ for a fixed value of r in an inner loop, the bisection algorithm iterates over r in an outer loop. The corresponding formulation is given by

$$r^* = \underset{r}{\text{argmax}}\{r : \mathcal{E}(\boldsymbol{\lambda}, r) \subseteq \mathcal{S}\} \tag{20}$$

which is a robustness analysis formulation in which the controller gains in $\boldsymbol{k}$ are fixed.

This approach is applied to determine the largest region centered at the origin, i.e., $e = \lambda_\alpha^2 + \lambda_q^2 - r^2 = 0$, for which the requirements $g_i(\boldsymbol{\lambda}, \boldsymbol{k}_{nom}) \leq 0$ for $i = 1, \ldots, 8$ introduced above are satisfied. Figure 5 shows the maximal set corresponding to the nominal controller.

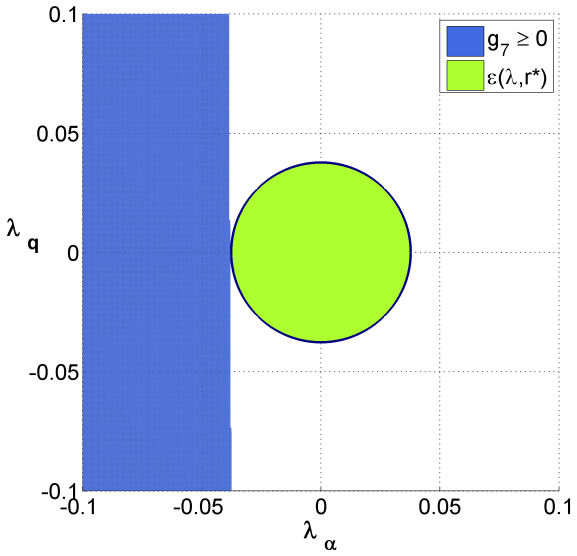

Figure 5. Region of constraint satisfaction and maximal set from SOS optimization.

The circle in Figure 5 represents a numerically proven lower bound on region of constraint satisfaction. The radius of this circle is $r^* = 0.037$, which implies that for all uncertainty values inside the circle, the closed-loop system is guaranteed to meet all performance and robustness requirements. It is important to note that SOS analysis is not guaranteed to provide a lower bound that is as "tight" as the results in Figure 5. Expanding the polynomial basis for $q(\boldsymbol{\lambda})$ is a potential remedy in this case. Each SOS evaluation is computed in about 2 seconds on a laptop with a dual-core processor and 4 GB of RAM. The SOS result shown in Figure 5 is found using a bisection algorithm with 10 iterations. Hence, the entire optimization was executed in about 20 seconds. The next section describes a method that takes advantage of SOS optimization to design an optimally robust controller.

V. Optimally Robust Control Design

A natural progression of the SOS optimization is to extend the method to controller synthesis. SOS optimization is useful in finding the maximal uncertainty set. Nonlinear optimization can be used in sequence with SOS analysis to identify the optimal gains yielding the largest maximal set. Nonlinear optimization

has the potential downside of converging to a non-global optimum. In this case, however, the consequence of such a result is less significant than in the uncertainty analysis case. The validity of the corresponding maximal set is guaranteed by the SOS optimization, although the gains may not correspond to the most robust controller allowed by the control structure. The formulation leading to the optimally robust controller gains is given by

$$\boldsymbol{k}^* = \underset{\boldsymbol{k}}{\text{argmax}}\{r^*(\boldsymbol{k})\} \tag{21}$$

where r^* is defined in Equation (20). The solution entails solving a nested optimization problem where the inner loop is an SOS problem in the coefficients of $q_i(\boldsymbol{\lambda})$, the middle loop is an optimization problem in the scalar radius r, and the outer loop is a nonlinear optimization in the controller gains $\boldsymbol{k}$.

This approach is used to tune the gains K_q and K_i of the controller in the X-15 aircraft example. The gain K_p is fixed at -1 to ensure that the PI controller only has an integral effect at low frequency. The optimal gains are found as $K_q = -1.26$ and $K_i = -1.58$, which (along with $K_p = -1$) constitute $\boldsymbol{k}^*$. Classical robustness in the outer loop is characterized by an infinite gain margin and a phase margin of 88.55 degrees. The revised gains have thus had little impact on the traditional metrics of robustness.

Figure 6 shows results corresponding to the optimally robust control design. The plot on the left shows the region of constraint satisfaction/violation in the uncertainty parameter space as well as the maximal set. The optimal radius of $r^*(\boldsymbol{k^*}) = 0.361$ is about 10 times larger than the nominal controller radius $r^*(\boldsymbol{k_{nom}}) = 0.037$. Note that the maximal set is limited by two conflicting requirements. In this case, the conflicting requirements are given by the tracking constraint $g_5(\boldsymbol{\lambda}, \boldsymbol{k^*}) \leq 0$ and the cross-over constraint $g_7(\boldsymbol{\lambda}, \boldsymbol{k^*}) \leq 0$. The cross-over constraint $g_8(\boldsymbol{\lambda}, \boldsymbol{k^*}) \leq 0$ is located nearby, although it is not active on the surface of the maximal set. The nonlinear optimization used to obtain this result converged in 729 seconds on the same laptop as described above, with 19 iterations and a total of 45 SOS bisections completed.

The plot on the right in Figure 6 shows the value of r^* as a function of the controller gains. The location of the peak on this plot corresponds to $\boldsymbol{k}^*$. This figure was obtained by solving the uncertainty analysis problem for a grid of points in the controller gain space. Due to the simplicity of the example, it is possible to grid the controller gain space and perform an SOS optimization at each grid point. The grid is refined near the peak to evaluate the convergence of the control design optimization. These results indicate that the manually tuned controller has significantly inferior robustness characteristics in comparison to its optimally robust counterpart.

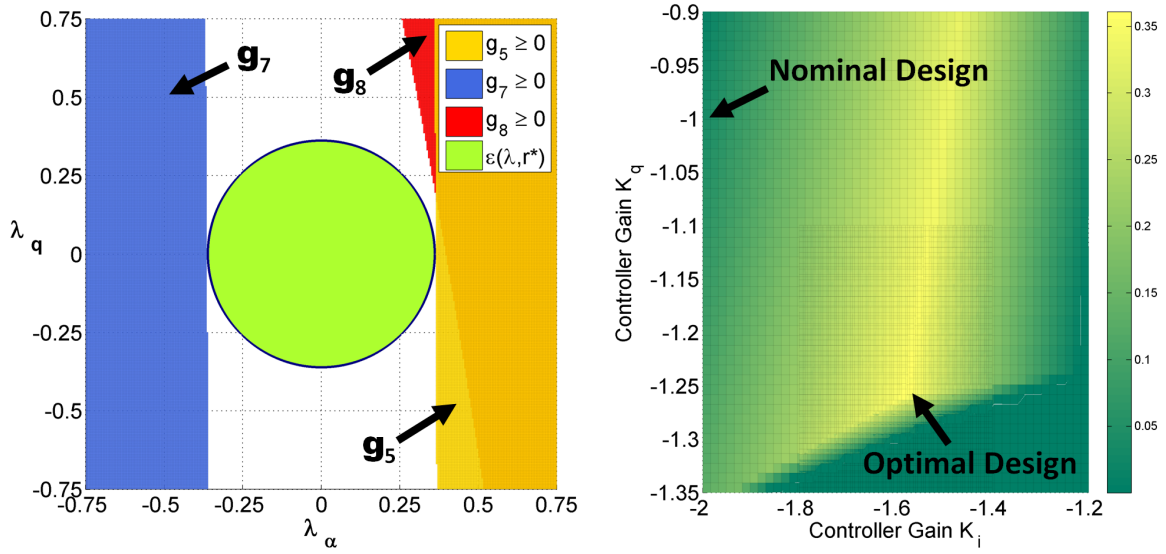

(a) Region of constraint satisfaction and maximal set.

(b) Topography of $r^*(\boldsymbol{k})$.

Figure 6. Graphical representation of the optimally robust control design.

The improved robustness of the optimal control design can also be examined in the frequency domain. For this analysis, uncertainty pairs are randomly selected from the maximal set corresponding to $\boldsymbol{k}^*$. Outer

loop transfer functions are generated with the selected uncertainty values for both the nominal and robust controller designs. Families of frequency responses are then generated accordingly. The results are shown in Figure 7, with the optimal control design on the left and the nominal on the right. Note that uncertainty values for which the optimally robust controller satisfies the requirements make the nominal controller violate constraint $g_7(\boldsymbol{\lambda}, \boldsymbol{k}_{nom}) \leq 0$. As indicated previously by the results in Figure 5, constraint function $g_7(\boldsymbol{\lambda}, \boldsymbol{k}_{nom})$ is violated if the radius of a candidate compliance region exceeds 0.037. The result on the left confirms that the optimally robust controller complies with the requirements for all the samples within $\mathcal{E}(\boldsymbol{\lambda}, r^* = 0.361)$.

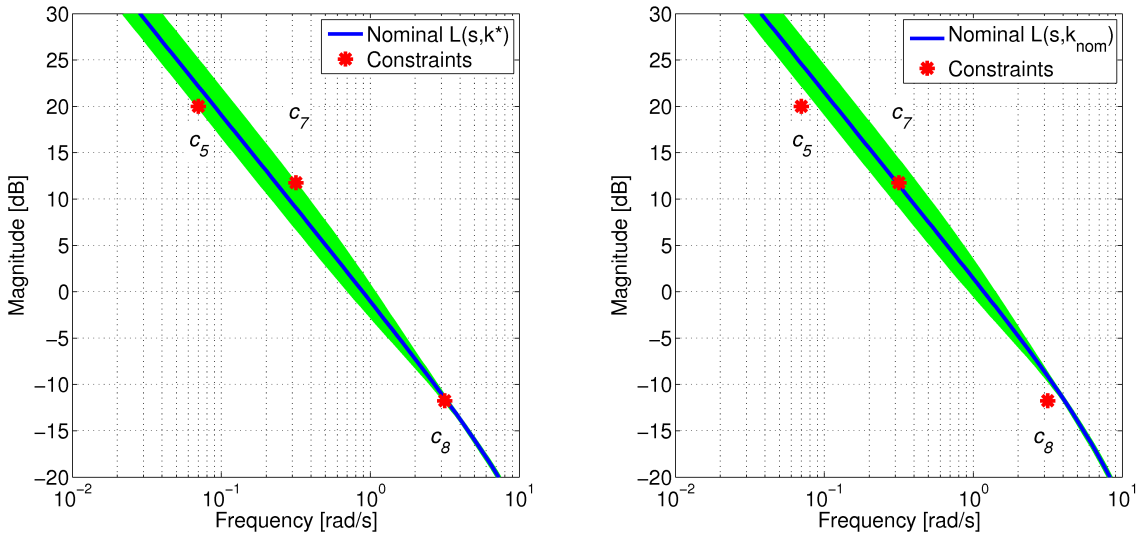

(a) Optimal outer loop transfer function with constraints. (b) Nominal outer loop transfer function with constraints.

Figure 7. Robustness of optimal design vs. nominal design with uncertainties from optimal maximal set.

VI. Conclusions

Sum-of-squares optimization is used to identify a range of parametric uncertainty for which a closed-loop system satisfies a set of stability and performance requirements. Nonlinear optimization is used in sequence with sum-of-squares analysis to obtain controllers that exhibit maximal robustness to parametric uncertainty. This method provides a novel approach for improving the robustness of controllers subject to parametric uncertainty and requirements that depend polynomially on the uncertainty.

Acknowledgments

This research was performed in collaboration with the Dynamic Systems & Control Branch at NASA Langley Research Center. The authors would like to thank the Langley Aerospace Research Summer Scholar (LARSS) program for funding this research.

References

[1]Skogestad, S. and Postlethwaite, I., *Multivariable Feedback Control*, John Wiley and Sons Ltd., 2007.

[2]Parrilo, P., *Structured Semidefinite Programs and Semialgebraic Geometry Methods in Robustness and Optimization*, Ph.D. thesis, California Institute of Technology, 2000.

[3]Crespo, L. G., Kenny, S. P., and Giesy, D. P., "A Computational Framework to Control Verification and Robustness Analysis," Tech. Rep. TP 2010-216189, NASA, 2010.

[4]Crespo, L. G., Kenny, S. P., and Giesy, D. P., "A Verification-Driven Approach to Control Analysis and Tuning," *AIAA Guidance Navigation and Control Conference*, No. AIAA-2008-6340, 2008.

[5]Annaswamy, A., Jang, J., and Lavretsky, E., "Stability margins for adaptive controllers in the presence of time delay," *AIAA Guidance, Navigation, and Control Conference*, No. AIAA 2008-6659, 2008.

[6]Cook, M., *Flight Dynamics Principles*, Elsevier Ltd., 2007.

[7]Ogata, K., *Modern Control Engineering*, Prentice Hall, 4th ed., 2002.

[8]Zettler, M. and Garloff, J., "Robustness analysis of polynomials with polynomial parameter dependency using Bernstein expansion," *IEEE Transactions on Automatic Control*, Vol. 43, No. 3, 1998.

[9]Powers, V. and Wormann, T., "An Algorithm for sums of squares of real polynomials," *Journal of Pure and Applied Algebra*, Vol. 127, 1998, pp. 99–104.

[10]Prajna, S., Papachristodoulou, A., Seiler, P., and Parrilo, P. A., *SOSTOOLS: Sum of squares optimization toolbox for MATLAB*, 2004.

[11]Balas, G., Packard, A., Seiler, P., and Topcu, U., "Notes from workshop at NASA Langley Research Center: Robustness Analysis of Nonlinear Systems," http://aem.umn.edu/∼AerospaceControl/.

[12]Lofberg, J., "YALMIP : A Toolbox for Modeling and Optimization in MATLAB," *Proceedings of the CACSD Conference*, Taipei, Taiwan, 2004.

[13]Sturm, J., "SeDuMi version 1.05," http://fewcal.kub.nl/sturm/software/sedumi.html, 2001.

[14]Sturm, J., "Using SeDuMi 1.02, a MATLAB toolbox for optimization over symmetric cones," *Optimization Methods and Software*, 1999, pp. 625–653.

[15]Crespo, L. G., Munoz, C. A., Narkawicz, A., Kenny, S. P., and Giesy, D. P., "Uncertainty Analysis via Failure Domain Characterization: Polynomial Requirement Functions," *ESREL Conference*, 2011.